Probing the Out-of-Plane Distortion of Single Point Defects in Atomically Thin Hexagonal Boron Nitride at the Picometer Scale

Nasim Alem, Oleg V. Yazyev, Christian Kisielowski, P. Denes, Ulrich Dahmen, Peter Hartel, Maximilian Haider, Maarten Bischoff, Bin Jiang, Steven G. Louie, and A. Zettl

Phys. Rev. Lett. **106**, 126102 — Published 21 March 2011

DOI: 10.1103/PhysRevLett.106.126102

Probing the Out-of-Plane Distortions to Single Point Defects at the Picometer Scale in Atomically Thin Hexagonal Boron Nitride

Nasim Alem,[1,2,3] Oleg V. Yazyev,[1,3] Christian Kisielowski,[3,4] P. Denes,[5] Ulrich Dahmen,[3,4] Peter Hartel,[6] Maximilian Haider,[6] Maarten Bischoff,[7] Bin Jiang,[8] Steven G. Louie,[1,3] and A. Zettl[1,2,3]

[1]*Department of Physics, University of California, Berkeley, California 94720, USA*
[2]*Center of Integrated Nanomechanical Systems, University of California, Berkeley, California 94720, USA*
[3]*Materials Sciences Division, Lawrence Berkeley National Laboratory, Berkeley, California 94720, USA*
[4]*National Center for Electron Microscopy, Lawrence Berkeley National Laboratory, Berkeley, California 94720, USA*
[5]*Engineering Division, Lawrence Berkeley National Laboratory, Berkeley, California 94720, USA*
[6]*CEOS GmbH, Englerstr. 28, D-69126 Heidelberg, Germany*
[7]*FEI Company, PO Box 80066, 5600 KA Eindhoven, The Netherlands*
[8]*FEI Company, NE Dawson Creek Dr., Hillsborow, OR*

Crystalline systems often lower their energy by atom displacements from regular high-symmetry lattice sites. We demonstrate that such symmetry lowering distortions can be visualized by ultra-high resolution transmission electron microscopy even at single point defects. Experimental investigation of structural distortions at the mono-vacancy defects in suspended bilayers of hexagonal boron nitride (h-BN) accompanied by first-principles calculations reveals a characteristic charge-induced pm-symmetry configuration of boron vacancies. This symmetry breaking is caused by interlayer bond reconstruction across the bilayer h-BN at the negatively charged boron vacancy defects and results in local membrane bending at the defect site. Therefore, the electron scattering potential is locally altered allowing for an experimental distinction between boron and nitrogen vacancies. This study confirms that boron vacancies are dominantly present in the h-BN membrane.

PACS numbers: 68.37.Og, 61.72.-y, 61.50.Ah, 42.15.Fr

Crystals can minimize their energy via bond distortions at the picometer scale [1–9]. Such distortions displace the atoms leading to a reduction of lattice symmetry either within the crystal lattice or locally at impurity or defect sites. Examples are charge density waves, where the displacements are driven by electron-phonon interactions or the Jahn-Teller effect, where the atom displacements lift the degeneracy of energy levels by lowering the crystal symmetry. Symmetry-breaking distortions have been reported in many crystals and molecular systems [2, 3, 10–13] including semiconductors [14], perovskites [2, 12], and high-T_C superconductors [3]. Such distortions can be driven by spin-spin, spin-lattice or Coulomb interactions and add a rich variety of effects to physics and chemistry. Knowledge of the atomic and electronic structure of point defects is very desirable, since they determine the material properties at the macroscopic scale. It has remained challenging, however, to directly image such effects since single atom sensitivity is required to probe the atomic displacements at the picometer scale.

In this Letter, we analyze the atomic displacements around point defects in hexagonal boron nitride (h-BN). h-BN consists of sp^2-bonded alternate boron and nitrogen atoms in a honeycomb structure [15–18]. In a recent study, boron and nitrogen sublattices in h-BN were unambiguously identified [15, 18]. In agreement with recent predictions [19], this identification showed that the majority of mono-vacancies produced by the 80 kV electron beam are formed as a result of removing a boron atom from the lattice. Nevertheless, no understanding of the local three dimensional structural distortions at the picometer length scale around such defects has been achieved. Such structural distortions are important since they determine the large-scale physical and electronic properties of crystals.

We use advanced sub-Ångstrom transmission electron microscopy (TEM) imaging, supported by first-principles calculations, to determine the three-dimensional structure of single mono-vacancies in a bilayer of h-BN. For this investigation, the TEAM I microscope [20] that cor-

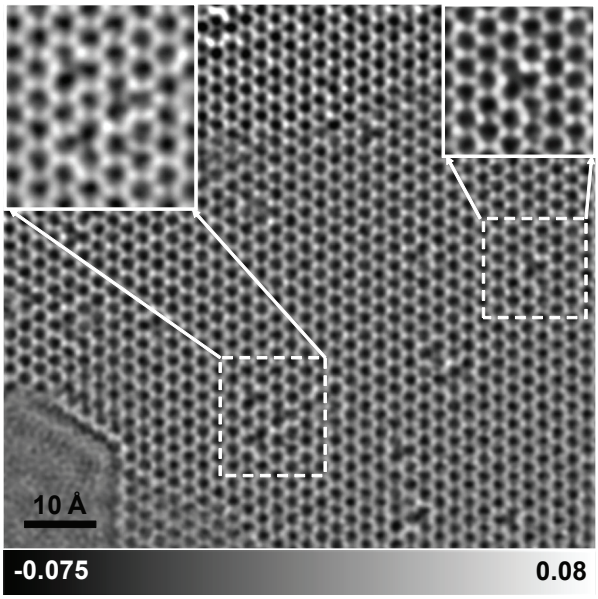

FIG. 1: Reconstructed phase of a bilayer h-BN imaged by the TEAM I microscope. The magnified inset images show broken symmetry at the defect sites. Color bar shows the relative phase in radians.

TABLE I: Relative energies ΔE of asymmetric boron vacancy configurations calculated with respect to the symmetric configurations in monolayer and bilayer h-BN and for different possible defect charge states $q = -2$ and $q = -3$.

	ΔE (eV)	
	monolayer h-BN	bilayer h-BN
$q = -2$	-0.05	-0.31
$q = -3$	-0.08	-0.62; -1.01

rects for both spherical and chromatic aberrations is utilized [21]. Figure 1 shows the reconstructed phase of the electron exit wave function [22] obtained from a focal series of h-BN images. The periodic bright contrast represents individual atoms/atom columns in h-BN that appear on a dark vacuum background. The small triangular features are the vacancies produced after ejection of atoms by the electron beam.

In bilayer h-BN, mono-vacancies can form on either the top or the bottom layer in the sample. After ejection of an atom from the lattice, it is expected that the three under-coordinated edge atoms will form a three-fold symmetric vacancy with a plane $p3$-symmetry in the projection of an image. Instead, we observe [the inset images in Fig. 1] a reduced pm-symmetry due to an unknown reconstruction mechanism. The asymmetric defects in h-BN are very stable under the 80 kV electron beam and exhibit a lifetime comparable to the acquisition time of the obtained focal series ($t = 10$ s, total electron dose 4.8×10^5 $e^-/\text{Å}^2$). Maintaining structural integrity for such a long time suggests that the asymmetric defect formation energy is of an order of electron-volt higher than the formation energy for the symmetric $p3$-configuration.

The reconstruction in h-BN differs from the reconstruction observed for mono-vacancies in graphene. The reconstruction of the vacancies in graphene is driven by the formation of a covalent bond between two under-coordinated carbon atoms at the vacancy edge [23, 24]. For h-BN, in contrast, covalent bond formation is not observed between the under-coordinated edge atoms. Instead, the contrast of the B–N columns at the edge of the mono-vacancies fluctuates significantly above the background in the defect-free region. In addition, the space between the central (missing) atom and the adjacent atom columns shows a gray level modulation/asymmetry reflecting the presence of a single mirror plane.

To understand the origin of the symmetry breaking, we performed first-principles calculations of boron and nitrogen mono-vacancies in mono- and bilayer h-BN [21]. All relevant charge states of the defects have been considered. Table I lists the calculated energies for the possible asymmetric configurations relative to the non-distorted symmetric configurations (ΔE) for boron mono-vacancies. Stable asymmetric configurations are predicted only for $q = -2$ and $q = -3$ charge states of boron vacancies in both mono- and bilayer h-BN. In a monolayer of h-BN, the relative energies for the asymmetric configuration are

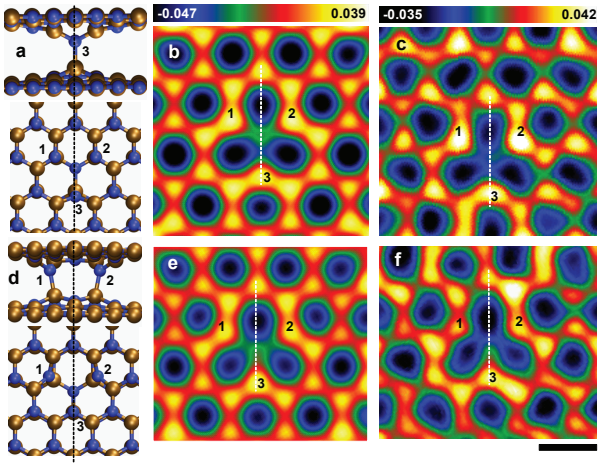

FIG. 2: (color online). Atomic structure models and phase of distorted boron mono-vacancies in bilayer h-BN with one and two interlayer bonds. (a, d) The top and cross-sectional view of stable defect configurations predicted from first principles showing in-plane and out-of-plane asymmetric distortions at the boron mono-vacancy with one and two B–N interlayer bonds. (b, e) A reconstructed phase, simulated from the models shown in (a) and (d) respectively. (c, f) Reconstructed phase of two mono-vacancies in a bilayer h-BN recorded on the TEAM I microscope. Color gradient represents the relative phase of the atoms (yellow indicates individual atoms; black corresponds to the centers of hexagons in the honeycomb lattice). The atoms are numbered for the ease of identification. The single mirror plane across the mono-vacancies is shown by white dashed lines. The scale bar is 2.5 Å. Color bar shows the relative phase in radians.

only -0.05 eV and -0.08 eV for the respective charge states. In contrast, for bilayer h-BN we find significantly larger energy differences due to the formation of B–N interlayer covalent bonds. In particular, two asymmetric configurations in the $q = -3$ charge state exhibit one and two out-of-plane interlayer covalent bonds [Fig. 2] resulting in $\Delta E = -0.62$ eV and $\Delta E = -1.01$ eV, respectively. The predicted B–N distances for the interlayer covalent bonds are 161 pm and 164 pm, respectively, introducing local *in-plane* and *out-of-plane* atom displacements at the local boron mono-vacancy sites. For such a bond formation, each participating atom shifts along the z direction by 1.1 Å, while the in-plane displacement of just below 0.4 Å is predicted in the direction opposite to the vacancy center. The calculations also predict a stable symmetric configuration ($\Delta E = -0.58$ eV) with all three nitrogen edge atoms forming interlayer covalent bonds.

The predicted distortion of the boron mono-vacancies in bilayer h-BN can be promoted by the two following driving forces: the Jahn-Teller distortion due to the electronic degeneracy of partially filled defect states, and the Coulomb repulsion effects in the highly charged defect configurations. While Jahn-Teller distortion can be realized for only intermediate charge states, the strongest distortion effects are predicted for the highest possible charge $q = -3$. Therefore, we conclude that Coulomb interaction is the dominant factor leading to the observed

structural distortion.

Unlike boron mono-vacancies, the predicted potential energy surfaces for nitrogen mono-vacancies do not have sufficiently stabilized asymmetric configurations for both monolayer and bilayer h-BN. No interlayer B–N bond formation was observed in our calculations, and the lifetime of individual distorted configurations is estimated to be orders of magnitude shorter than the recording time [21].

Recent studies show that the position of atoms can fluctuate on the time scale of the image exposure (0.5–1 s) in atomically thin membranes [15, 25, 26]. To identify the structural distortions at the mono-vacancies, such beam-induced vibrations should be carefully evaluated. We have estimated the in-plane beam-induced vibration of 50 to 65 pm at full-width half-maximum (FWHM) in a defect-free region of the h-BN [Ref. 21, Sec. V]. Although the predicted in-plane distortions at the vacancy sites (≈40 pm) fall within the estimated beam-induced vibrations, first-principles calculations predict significantly higher out-of-plane distortions (≈110 pm) at the mono-vacancies. Here we use the out-of-plane distortions to verify the broken symmetry at the mono-vacancy sites.

Figure 2 compares the TEAM I reconstructed phase and the simulated phase of the two stable asymmetric boron vacancy configurations at $q = -3$ [21]. Formation of the out-of-plane interlayer bonds across bilayer h-BN results in reduced pm-symmetry of boron mono-vacancies and leads to an observable contrast gradient and geometry at the corners of each mono-vacancy in the simulated and TEAM I images. In addition, the atomic columns at the vacancy perimeter exhibit significantly large intensities well above the background.

To determine the displacements along the z axis, the scattering potential of the atomic columns, leading to such a phase modulation, should be assessed. Van Dyck *et al.* [27] show that the phase of the electron exit wave function is modulated by the strength of the scattering centers as well as the atomic spacing along the column. This relation is verified by multi-slice calculations for an isolated B–N pair [Ref. 21, Fig. S5]. According to this relation the phase increases with decreasing atom spacing and decreases when lateral displacements are introduced to the atoms. This relation is used to assess the structural distortions at the vacancy sites. In principle, the alteration of charge density contributes to the phase changes. However, in our particular case the phase changes are dominated by atom displacements and the residual lens aberrations [21, 28].

To evaluate the phase shift at the vicinity of the vacancies, we have estimated the inter-atomic distance across the bilayer h-BN from the phase of each individual atom column at each defect site [Fig. 3]. The two simulated solid and dashed curves in Fig. 3 illustrate the effect of inter-atomic distance on the resulting phase for a B–N pair [Ref. 21, Fig. S5]. We have measured the phase of each individual atom column at the perimeter of the

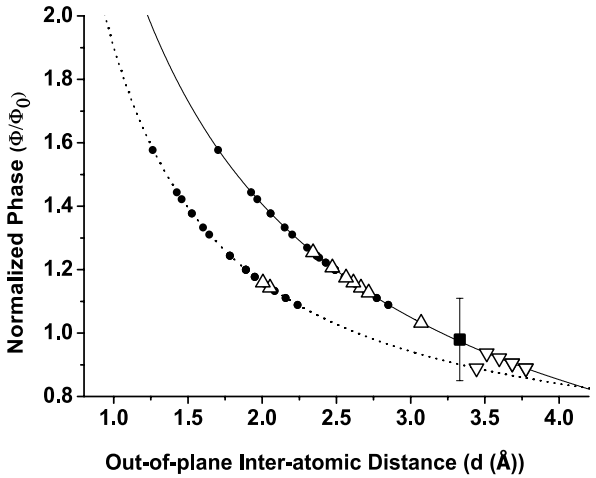

FIG. 3: Normalized phase of the exit wave as a function of out-of-plane inter-atomic distance for each individual atom column at the vacancy perimeter for the simulated and the TEAM I images in bilayer h-BN. The phase in the defect-free region of bilayer h-BN is normalized to unity. The two solid and dashed curves show the normalized phase versus the out-of-plane distance for a simulated B–N pair with no in-plane (solid line) and 35 pm in-plane (dashed line) distortion. Normalized phase for each individual atom column at the perimeter of the simulated boron (△) and simulated nitrogen (▽) mono-vacancies is projected on the solid and dashed lines. The data points projected on the dashed line correspond to atom columns at the vacancy edge atoms with in-plane distortion. TEAM I atom columns at the perimeter of the mono-vacancies (•) are projected on both the solid and dashed lines, while TEAM I atom columns at the defect-free region (■) are projected on the solid line. The error bar corresponds to 13% variation in the magnitude of the phase shift in the defect-free region of the film.

mono-vacancies, previously shown in Fig. 2, and have attributed them to the inter-atomic distance across the bilayer. The individual data points projected on the curves present the estimated inter-atomic distance for each individual atom column at the mono-vacancies from their relative phase shift.

To further verify the local phase shifts around the vacancies in TEAM I images, we have subtracted the phase of a defect-free region of h-BN from a region containing a vacancy [Fig. 4(a)]. A significant phase shift can be observed around the vacancy in the resulting residual phase image [Fig. 4(b)]. The two Gaussian plots show a shift in the mean value of the residual phase around the vacancy with respect to the background [Fig. 4(c)]. This phase shift can also be observed in the line profile across the vacancy [Fig. 4(d)].

The significant phase shift at the atomic columns at the vacancy perimeter is attributed to the dependence of scattering potential on the atom spacing in the beam direction. This phase shift signifies the out-of-plane atom displacements and the local bending of the bilayer at the defect sites. Such large out-of-plane displacements are a clear signature of boron mono-vacancies, since no out-

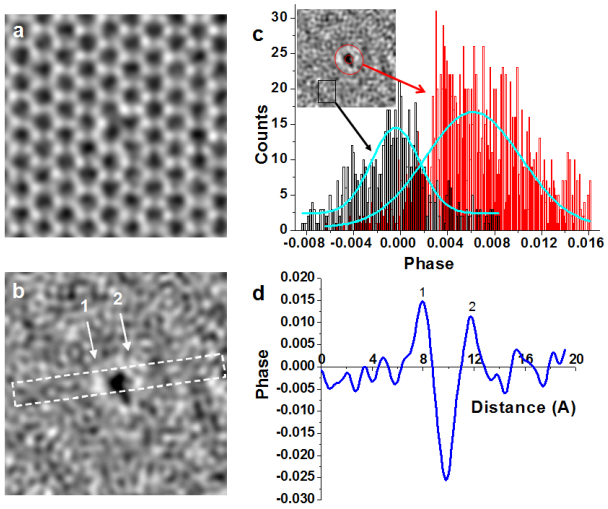

FIG. 4: (color online). (a) Phase of a mono-vacancy and (b) residual phase around the vacancy after the phase from the defect-free region is subtracted. (c) Distribution of residual phase showing a phase shift at the vicinity of the vacancy compared to the background. (d) Phase profile across the vacancy.

of-plane displacement is predicted to occur at nitrogen defect sites. For comparison, simulated boron and nitrogen mono-vacancies are projected in Fig. [3]. Simulated boron mono-vacancies show reduction in their interlayer bond distance, similar to the defects observed by TEAM I. In the case of simulated nitrogen vacancies, no reduction in the inter-layer bond is predicted and therefore no increase in the phase of the atomic columns is observed at the vacancy perimeter. Fig. 3 shows good agreement between the TEAM I and simulated boron mono-vacancies, if we consider the relative strength of the potential as well as the existing beam-induced vibrations in the film (50–65 pm at FWHM). Nitrogen vacancies do not form interlayer bonds and, thus, do not lead to observable increase in the magnitude of the phase at the vacancy perimeter. Therefore, we conclusively observe boron vacancies in the TEAM I images obtained in this experiment.

In conclusion, we reveal the structural distortions of the vacancy defects in bilayer *h*-BN by analyzing the three-dimensional atomic displacements employing ultra-high resolution electron microscopy in combination with first-principles calculations. To uncover such distortions in *h*-BN, we use aberration-corrected electron microscopy where both *spherical* and *chromatic* lens aberrations are corrected resulting in a high signal to noise ratio, single atom sensitivity, and sub-Ångstrom resolution. In bilayer *h*-BN, boron mono-vacancies can be identified because of the formation of out-of-plane covalent bonds across the *h*-BN bilayer. This is a charge state driven distortion and is only predicted to occur in boron mono-vacancies. *h*-BN bilayer membrane is locally bent at the boron defect sites resulting in a local symmetry reduction from *p*3- to *pm*-configuration at the boron defect sites. Understanding the mechanisms behind structural distortions in crystal membranes and molecular systems is at the heart of condensed matter phenomena, since it helps elucidate the physical properties of the material. Furthermore, imaging such distortions helps resolve the mechanisms behind local lattice distortions in the vacancy and interstitial sites as well as the mechanisms behind the functionalization of atomically thin sp^2-bonded membranes [29].

This work is supported by US DOE Contract DE-AC02-05CH11231 which provided for computational and theoretical analysis and preliminary TEM characterization. The Center of Integrated Nanomechanical Systems (COINS) with grant number EEC-0425914 provided for sample preparation. TEAM I imaging was performed at NCEM, which is supported by the Office of Science, Office of BES of the U.S. DOE under Contract No. DE-AC02-05CH11231. O.V.Y. acknowledges financial support of the Swiss NSF (grant No. PBELP2-123086). The computational resources have been provided by NSF through TeraGrid resources at NICS (Kraken).

[1] I. B. Bersuker, Chem. Rev. **101**, 1067 (2001).
[2] C. H. Booth *et al.*, Phys. Rev. B **57**, 10440 (1998).
[3] G. G. Sergeeva and A. A. Soroka, Low Temp. Phys. **30**, 667 (2004).
[4] A. Zobelli *et al.*, Nano Lett. **6**, 1955 (2006).
[5] S. Biermann *et al.*, Phys. Rev. Lett. **94**, 026404 (2005).
[6] W. Eerenstein, N. D. Mathur, and J. F. Scott, Nature (London) **442**, 759 (2006).
[7] R. H. Friend and D. Jerome, J. Phys. C **12**, 1441 (1979).
[8] A. J. Heeger *et al.*, Rev. Mod. Phys. **60**, 781 (1988).
[9] M. Wuttig and N. Yamada, Nature Mater. **6**, 824 (2007).
[10] T. Lingner *et al.*, Phys. Rev. B **64**, 245212 (2001).
[11] F. Negri, G. Orlandi, and F. Zerbetto, Chem. Phys. Lett. **144**, 31 (1988).
[12] J. Rodriguez-Carvajal *et al.*, Phys. Rev. B **57**, 3189 (1998).
[13] A. Wachowiak *et al.*, Science **310**, 468 (2005).
[14] E. Malguth *et al.*, Phys. Rev. B **74**, 165201 (2006).
[15] N. Alem *et al.*, Phys. Rev. B **80**, 155425 (2009).
[16] C. H. Jin *et al.*, Phys. Rev. Lett. **102**, 195505 (2009).
[17] J. C. Meyer *et al.*, Nano Lett. **9**, 2683 (2009).
[18] O. L. Krivanek *et al.*, Nature [0028-0836] Krivanek (2010), **464**,571 (2010).
[19] A. Zobelli **et al.**, Phys. Rev. B **75**, 245402 (2007).
[20] U. Dahmen *et al.*, Philos. Trans. R. Soc. London, Ser. A **367**, 3795 (2009).
[21] See supplementary material at [EPAPS URL].
[22] R. W. Gerchber *et al.*, OPTIK **35**, 237 (1972).
[23] A. A. El-Barbary *et al.*, Phys. Rev. B **68**, 144107 (2003).
[24] J. C. Meyer *et al.*, Nano Lett. **8**, 3582 (2008).
[25] D. Alloyeau *et al.*, Phys. Rev. B **80**, 014114 (2009).
[26] C. Kisielowski *et al.*, Angew. Chem., Int. Ed **49**, 2708 (2010).
[27] D. Van Dyck and J. H. Chen, Solid State Comm. **109**, 501 (1999).
[28] J.C. Meyer *et al.*, Nature Mater., advance online publication (doi: 10.1038/nmat2941).
[29] R. Erni *et al.*, Phys. Rev. B **80**, 165443 (2010).